Four-photon absorption cross section in potassium bromide at 532 nm

X. A. Shen, Scott C. Jones, and Peter Braunlich
Department of Physics, Washington State University, Pullman, Washington 99164-2814

Paul Kelly
National Research Council, Ottawa K1A 0R6, Canada
(Received 2 March 1987)

We exploit recombination luminescence of self-trapped excitons for the measurement of the four-photon absorption cross section in KBr at 532 nm. The value is found to be $\sigma^{(4)}=(2\pm1)\times10^{-112}$ $cm^8 sec^3$. The validity of this method is verified by comparison with a four-photon absorption model describing the interaction process.

I. INTRODUCTION

Transparent optical materials may absorb considerable energy from a high-power laser pulse and suffer irreversible modification in the process. An overwhelming number of observations of this so-called laser-induced optical breakdown reported in the literature are *extrinsic* in nature: The damage is caused by enhanced absorption due to imperfections (inclusions, lattice defects, impurities, etc.) Unequivocally documented measurements of optical breakdown as a result of the interaction between an *intrinsic* optical material and the laser photon field are rare and, as a consequence, the fundamental nature of this nonlinear interaction is not well understood despite an intensive research effort during the past two decades.[1–9] While theoretical models have been advocated early on,[3–5,8] experimental difficulties and the lack of sufficiently pure and perfect crystals have usually prevented direct comparison between theory and experiment.

A notable exception is the recent measurement of prebreakdown energy deposition from intense 80-ps laser pulses at 532 nm in specially purified NaCl by Jones *et al.*[10] who showed that the primary mechanism of absorption in this case is four-photon exciton generation and subsequent free-electron absorption with contributions from low-order absorption by laser-generated primary defects. Under these experimental conditions, not, as expected, impact ionization and electron-avalanche formation, but high-order multiphoton processes cause energy deposition from the laser pulse that is sufficient to increase the temperature in the interaction volume by hundreds of degrees Kelvin. As a result of this work, we must revise the previously held belief that in optical materials impact ionization will dominate multiphoton processes of order $m>2$.[1–6]

The newly discovered key role of higher-order multiphoton absorption in the mechanism of energy deposition from the laser beam to the transparent crystal reemphasizes the importance of reliable measurements of multiphoton absorption cross sections in solids. While an abundant literature exists of calculated and measured cross sections of order $m\leq3$, there is precious little trustworthy information available for $m>3$.[11] This motivated us to further measure four-photon cross sections in alkali halides. It is the purpose of this paper to report results obtained in KBr at 532 nm.

Although alkali halides are presently not used as high-power optical materials in the visible, we choose them for our investigation of the optical-breakdown mechanism because their optical, thermal, and mechanical properties are well known, and they are also ideal candidates for studying the role of laser-generated photochemical defects in the interaction with intense laser beams.

We exploit recombination luminescence of four-photon-generated self-trapped excitons (STE's) at about 50 K as a monitor of the processes which take place during the interaction of KBr with a 532-nm laser pulse. A similar method was first used in our laboratory by Brost *et al.*[12] for the measurement of the three-photon absorption cross section at 532 nm in KI. However, in order to extend this technique to a fourth-order absorption process in an alkali halide, considerable improvements had to be instituted, the two most effective being the replacement of the mode-locked pulse train by a single amplified pulse of 74 ps half-width at $1/e$ intensity and the design of a fiber-optics luminescence collection system. The former substantially reduced laser-induced defect absorption (e.g., by laser-generated STE's) which otherwise would affect the luminescence yield, while the latter substantially enhanced the luminescence collection efficiency. In fact, useful emission spectra were obtained at photon fluxes 1 order of magnitude smaller than those required for the detection of four-photon processes in NaCl with the photoacoustic technique described by Jones *et al.*[10]

Compared to photoacoustic detection of four-photon energy deposition in a transparent solid, the STE recombination luminescence method[12] requires separate calibration with respect to a luminescence signal produced by an exciton-generation process of known absorption cross section. In our case this is achieved by measuring the STE luminescence that results from two-photon generation of electron-hole pairs by 266-nm laser pulses. This cross section is taken from published data, and the calibration procedure rests on the assumption of equal quantum efficiencies of the STE luminescence per generated electron-hole pair under both 266- and 532-nm excita-

tions. However, as will be discussed below, this simple direct approach yields only a first-order approximation for the four-photon absorption cross section because it disregards the differences in the interaction of the laser-generated primary defects with photons of different wavelengths. A detailed analysis of the various defect-photon interaction processes is required to arrive at the correct value for the desired four-photon cross section.

II. FIRST-ORDER APPROXIMATION

The equation describing the transition rate of electrons from the valence band to the conduction band in a crystal under multiphoton excitation can be written as[13]

$$\frac{dn_c}{dt}=\sigma^{(m)}NF_m^m \ , \tag{1}$$

where n_c is the concentration of the conduction electrons generated under m-photon excitation, $\sigma^{(m)}$ the m-photon absorption cross section, N the density of the active atoms in the crystal (i.e., Br^- ions in our case), and F_m the incident photon flux for m-photon excitation. This transition results in the creation of one electron-hole pair per multiphoton absorption event of order m.

In alkali halides at low temperature one of the channels for relaxation of these pairs is formation of self-trapped excitons which decay to their ground state by emitting photons.[14] There are two STE emission bands in most alkali halides,[15] characterized by the polarization direction with respect to the molecular axis of the STE. The emission polarized parallel to the axis is known as σ luminescence and that polarized normal to the axis as π luminescence. This radiative relaxation of the electron-hole pairs allows us to relate the number of STE's (σ, π, or both) generated under m-photon excitation in alkali halides to the above rate equation. For example, the total STE luminescence L_m emitted from the interaction volume is obtained by integration over volume V and time t:

$$L_m=\int_V\int_{-\infty}^{\infty}\xi_m\sigma^{(m)}NF_m^m(\mathbf{r},t)dV\,dt \ . \tag{2}$$

Here ξ_m is the effective quantum efficiency for generating STE luminescence under the m-photon excitation. It is a product of two parts: (1) the intrinsic STE luminescence efficiency, that is the probability of emitting a luminescence photon per electron-hole pair, and (2) a modification factor introduced by the ionization and redistribution[12] of electrons over the various excited states of the STE's due to their interaction with laser photons. In our experiment, the first part is the same for both two- and four-photon cases, because the resulting transitions under both excitations obey the same selection rules (since m is an even integer) and lead to identical excited states (note the same total quantum energy of excitation of 9.32 eV). The second part requires careful consideration of the complex interaction of the m-photon–generated excitons and primary defects (e.g., STE's) with the incident laser pulses.

Since we monitor exclusively the luminescence emission from self-trapped excitons, we need be concerned only with transitions involving STE states. If the time of STE formation is short (less than the incident pulse duration), they may absorb photons during the interaction. Such photon absorption may result in ionization and/or redistribution and, as a consequence, affect the STE luminescence yield. This modification factor may, thus, depend strongly on the laser-photon flux and wavelength.

In first approximation, we assume that these effects are negligible and treat ξ_m simply a constant ξ. A detailed analysis of the influence of the STE-photon interaction on luminescence yield and, thus, on the measured four-photon cross section is presented in Sec. V. It will be shown there that the approximation is indeed a good one in the case of KBr exposed to short, intense laser pulses at 532 nm.

The measurable luminescence signal is limited by the collection efficiency η_m which is determined by the experimental setup as well as the order of the multiphoton process. The reason for the latter can be easily seen from Eq. (2). Under otherwise identical experimental conditions, a change of order m will result in changing the spatial distribution of the STE luminescence intensity.

By measuring the STE luminescence signals generated under both four- and two-photon excitation as a function of the respective photon fluxes together with the characteristic parameters of the excitation pulses, we obtain a first-order approximation of the four-photon absorption cross section via the expression

$$\sigma^{(4)}=\sigma^{(2)}\frac{\eta_2 L_4\int\int NF_2^2dV\,dt}{\eta_4 L_2\int\int NF_4^4dV\,dt} \ . \tag{3}$$

III. EXPERIMENTAL ARRANGEMENT AND PROCEDURE

A schematic diagram of the experimental arrangement is given in Fig. 1. The laser system consists of a Quantronix model 116 Q-switched and mode-locked Nd:YAG laser (where YAG stands for yttrium aluminum garnet), a pulse selector, and a Quantel Nd:YAG double-pass amplifier. The Quantronix Nd:YAG laser generates a Q-switched pulse train at 1064 nm. A single mode-locked pulse is selected by the pulse selector and subsequently amplified with a gain of about 1000. The second-harmonic generator, a potassium-dideuterium phosphate (KD*P) crystal, converts the amplified pulse at 1064 to 532 nm with a conversion efficiency around 60%. The 532-nm pulse is then divided with a 50-50 beam splitter. One of the pulses passes through a second frequency doubler (fourth-harmonic generator) which converts 30% of its energy to 266 nm. The two beams (532 and 266 nm) are carefully aligned so that they properly overlap at the sample position. During an experimental run, one of the beams is always blocked. A 1-in.-diameter uv fused-silica planoconvex lens (with focal lengths of 66.6 mm at 532 nm and 61.4 mm at 266 nm) is used to focus either 532- or 266-nm pulses in a KBr sample. The polarization of the incident laser pulses is along the $\langle 110\rangle$ direction of the sample. The pulse energy at both wavelengths is monitored by photodiodes, which are calibrated against an energy meter for pulse energy delivered to the sample.

The samples are reactive-atmosphere–processed (to reduce concentration of OH^-) ultrapure KBr single crystals obtained from the University of Utah. They are

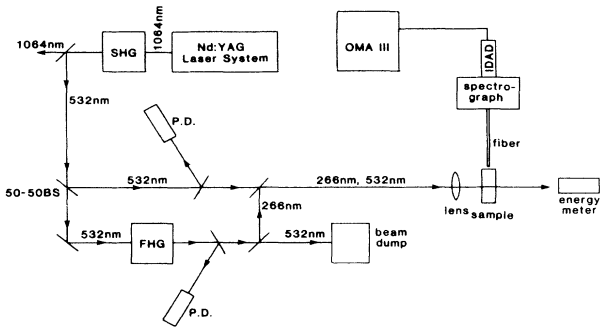

FIG. 1. Schematic diagram of the experimental arrangement for the measurement of the four-photon absorption cross section in KBr. The laser system, triggered by an optical multichannel analyzer (OMA III), produces single 1064-nm mode-locked pulses which are converted to 532 nm by a second harmonic generator (SHG). A dichroic beam splitter transmits the residual 1064-nm laser light and reflects the 532-nm pulse to a 50-50 beam splitter (50-50BS) which divides the pulse into two. The fourth-harmonic generator (FHG) converts one pulse to 266 nm. The two beams of different wavelengths are reunited with two dichroic beamsplitters. The energy of the incident pulses is monitored by two photodiodes (PD) with the aid of two partially reflective mirrors. A uv fused-silica lens focuses the laser pulses into a KBr sample with their polarization parallel to the $\langle 110 \rangle$ direction of the sample. The σ luminescence signals generated under both 266- and 532-nm excitations are collected by a uv-grade fiber and are detected by the OMA with an intensified diode array detector (IDAD).

mounted vertically on a cold finger in a closed-cycle refrigerated optical cryostat operated at temperatures around 50 K. The vessel is evacuated to 10^{-6} Torr at room temperature. The sample size is approximately $4\times4\times25$ mm^3. The cold finger and sample are movable in the plane perpendicular to the laser-beam axis so that different sites can be chosen in the crystal without affecting the efficiency of collecting luminescence photons. The front and back surfaces of all samples are cleaved. Reflection losses per surface are determined to be approximately 5% and 15% for 532- and 266-nm laser light, respectively.

Using the second-harmonic-generation autocorrelation method,[16] the temporal profile of the 532-nm pulse is measured to be approximately Gaussian with a halfwidth $\tau_g = 74$ ps at $1/e$ intensity. From the properties of second-harmonic generation[17] the temporal pulse width for the 266-nm pulse τ_{uv} is assumed to be equal to $\tau_g/\sqrt{2}$. The spatial distributions of the two beams at the focal point are calculated from the respective beam diameters at the lens-input surface using diffraction-limited optics. The diameters are measured at the focusing lens position with the slit-scanning technique (similar to the knife-edge technique,[18] but with a slit of a few micrometers width instead). Typical spot sizes obtained at the focal point are between 4 and 9 μm in radius at $1/e$ intensity.

We disregard here beam deformation caused by self-focusing or defocusing for the following reasons. Soileau *et al.*[19] have shown that for a tightly focused 532-nm beam (beam waist between 3.4 and 14 μm half width at $1/e$ intensity) the self-focusing effect does not occur in NaCl (with similar nonlinear optical properties as KBr) at photon fluxes up to the damage threshold. These authors demonstrate this by examining the polarization dependence of the breakdown threshold and the distortion of the transmitted beam, and conclude that self-focusing is not important under the condition of tightly focused laser beams.[19] Further, our experimental results indicate the absence of self-focusing because the measured dependence of the luminescence intensity on incident pulse energy follows predictions from detailed model calculations without the need to consider beam deformation (see below). If self-focusing were present, one would expect the slope of a plot of STE luminescence versus incident pulse energy on a log-log scale to be steeper than 4 in the four-photon case. Similar arguments apply to beam defocusing due to reduction of the refractive index by multiphoton-generated free carriers, which would reduce this slope. We show below that the observed deviation from slope 4 is entirely caused by STE-photon interaction and that any other conceivable contribution (including a rise in temperature) is absent. Jones *et al.*[10] have reached a similar conclusion in their work on nonlinear energy deposition by four-photon absorption of NaCl at 532 nm.

The induced STE luminescence signals are collected by a single uv-grade quartz fiber of 1-mm diameter. The luminescence spectrum is recorded with an EG&G model 1460 optical multichannel analyzer (OMA III) with an intensified diode array detector and a spectrograph. A typical STE luminescence spectrum from KBr obtained with single-laser-pulse excitation at 266 nm is shown in Fig. 2. The position of the fiber is adjustable horizontally along the beam path and perpendicular to it. This facilitates proper positioning of the fiber with respect to the sample for optimization of the collection efficiency.

To insure that the focal points for both 532- and 266-nm pulses are exactly on the axis of the fiber, the STE luminescence signals under both excitations are monitored and maximized by moving the lens along the beam axis. The final arrangement of the fiber and the sample is shown in Fig. 3. The luminescence collection efficiency

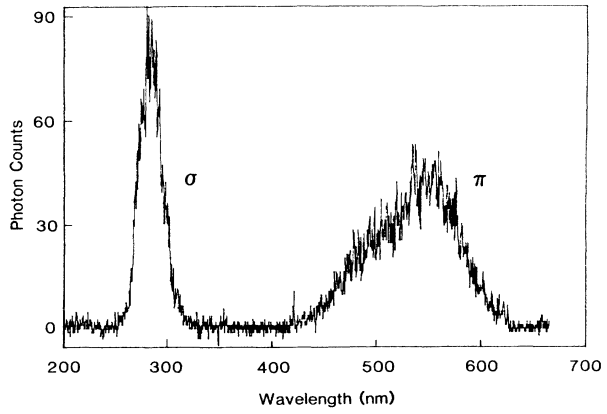

FIG. 2. STE luminescence spectrum in KBr obtained at 50 K with single-pulse excitation at 266 nm.

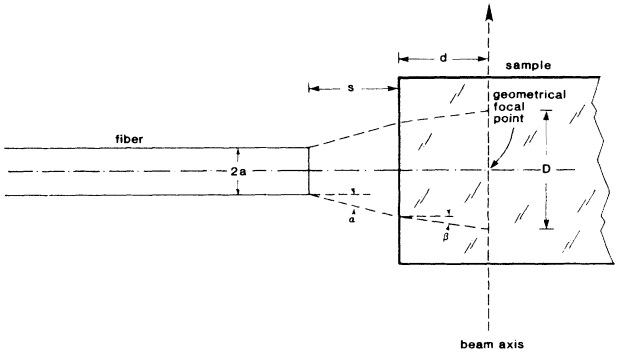

FIG. 3. Arrangement of the fiber with respect to the sample position and the beam axis. The focal points of both 266- and 532-nm laser light are positioned on the axis of the fiber. The critical angle α and the interaction length D are determined by the numerical aperture of the fiber.

for the fiber is then calculated based on this geometry (see Appendix A).

Because the π luminescence overlaps the 532-nm incident laser light, it is difficult to accurately measure very weak π-luminescence signals under intense 532-nm excitation. Therefore, we utilized only the σ luminescence for the measurement of the four-photon absorption cross section in KBr. The use of the σ luminescence also excludes the possibility of detecting π luminescence induced by a dipole-allowed three-photon excitation of free excitons.[15]

The experiment is conducted as follows. With the arrangement discussed above, the luminescence is induced by exposing the sample to a single 532-nm pulse and detected by the OMA. The total integrated σ luminescence collected per laser pulse is recorded. To ensure that data are taken from virgin material, a new interaction site in the sample is chosen after each pulse. By varying the energy of the laser pulse, a relationship between luminescence yield and laser photon flux is obtained. The same process is repeated for the two-photon measurement.

Since the typical laser beam waists at the focal point are between 4 and 9 μm in radius, the interaction volume can be treated as a line source for purposes of performing the integrations in Eq. (3) and calculating the luminescence collection efficiencies. Therefore, the integration limits for the volume integral in Eq. (3) can simply be taken to be infinity in the radial direction and are otherwise limited to the diameter D of the acceptance cone of the fiber (determined by the numerical aperture of the fiber, A_N, in our case $A_N=0.2$, and the fiber diameter). This limit can be obtained from Fig. 3. It is

$$D=2a+2\left[s\tan\alpha+\frac{d\sin\alpha}{(n^2-\sin^2\alpha)^{1/2}}\right],$$

where a is the radius of the fiber, n the refractive index of the sample, $\alpha=\sin^{-1}(A_N)$, and s and d are given in the figure.

By using Gaussian spatial and temporal profiles for the laser pulses, that is

$$F(\mathbf{r},t)=F_0\frac{w_0^2}{w^2(z)}\exp\left[-\frac{r^2}{w^2(z)}-\frac{t^2}{\tau^2}\right],$$

with

$$w^2(z)=w_0^2\left[1+\left[\frac{z}{z_0}\right]^2\right],$$

and converting photon fluxes to total energy, we can simplify the expression [Eq. (3)] for $\sigma^{(4)}$ to

$$\sigma^{(4)}=\frac{\pi^3}{2\sqrt{2}}\sigma^{(2)}(\hbar\omega_g)^2\frac{\eta_2\tau_g^3}{\eta_4\tau_{uv}}\frac{w_{0g}^8}{w_{0uv}^4}\frac{(L_4/E_4^4)}{(L_2/E_2^2)}\frac{V_{uv}}{V_g}, \quad (4)$$

where

$$V_g=\frac{\pi}{2}w_{0g}^2z_{0g}\left[\frac{(D/2z_{0g})}{4[1+(D/2z_{0g})^2]^2}+\frac{3(D/2z_{0g})}{8[1+(D/2z_{0g})^2]}+\tfrac{3}{8}\tan^{-1}\left[\frac{D}{2z_{0g}}\right]\right]$$

and

$$V_{uv}=\pi w_{0uv}^2z_{0uv}\tan^{-1}\left[\frac{D}{2z_{0uv}}\right].$$

Here E_m is the total incident laser pulse energy for m-photon excitation, $\hbar\omega_g$ the photon energy at 532 nm, w_0 the Gaussian beam waist, z_0 the confocal parameter, τ the pulse width at $1/e$ intensity, V the fraction of the interaction volume visible to the fiber, and the subscripts g and uv denote those parameters at 532- and 266-nm wavelengths, respectively. This expression is the one used in the calculation of the four-photon absorption cross section for KBr, whereby the required two-photon absorption cross section $\sigma^{(2)}$ is taken from Liu *et al.*[20]

IV. EXPERIMENTAL RESULTS

The dependence of the measured STE luminescence intensity on the incident pulse energy at 532 nm is shown in Fig. 4. The σ-luminescence yield exhibits a nearly fourth-order dependence on the incident pulse energy, indicating the primary exciton generation process is four-photon absorption. As will be shown in the following section, a slope of slightly less than 4 is expected. This deviation from slope 4 is attributed to STE absorption at very high photon fluxes ($>10^{29}$ photons/cm^2 sec at the peak of the pulse) at which the STE's ionize and/or are redistributed among themselves (see following section). Having, thus, experimentally confirmed that the electron-hole–pair

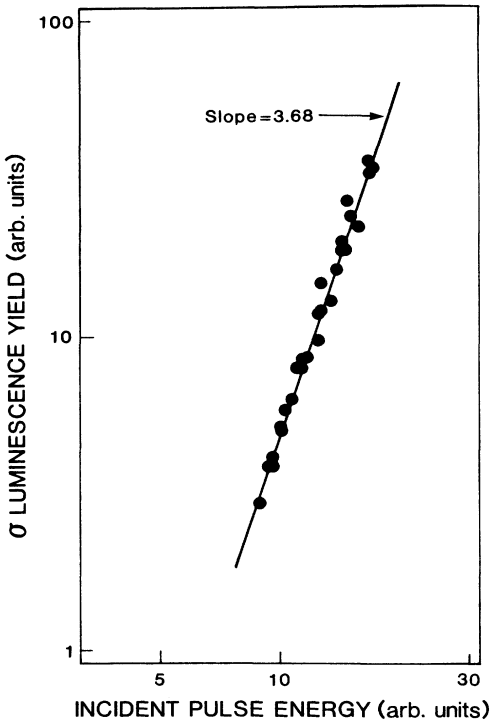

FIG. 4. Double-logarithmic plot of σ luminescence yield versus incident pulse energy at 532 nm. The slope of nearly 4 indicates that the primary exciton generation process is four-photon absorption.

generation process is indeed four-photon absorption, we are justified in determining the four-photon absorption cross section according to the method described in Secs. II and III. The results are listed in Table I.

Here we report on measurements using four crystals from two different parts of one boule. The consistency of the results is very good for such high-order nonlinear absorption processes. A slight variation (a factor of 8 at most) of $\sigma^{(4)}$ is possibly due to the differences in the impurity and defect concentrations of the samples, as it is known that the impurity content of a crystal pulled from the melt increases as it grows. Thus, it tends to be "cleaner" on top than at the bottom. The results obtained from the same part of the boule confirm this by yielding consistent values for $\sigma^{(4)}$. The fact that less pure crystals yield smaller cross sections remains to be explained. The equally weighted average value of the four-photon section is $(2\pm1)\times10^{-112}$ cm^8 sec^3, which is approximately 2 orders of magnitude larger than that measured by Catalano *et al.*[21] using a ruby laser at 693 nm.

An error analysis indicates that the main contribution to the uncertainty of $\sigma^{(4)}$ stems from the accuracy of the pulse energy measurement, which is traceable to a secondary standard to within 5%. This, together with the accuracy of the electronics, yields an overall uncertainty of E_m of approximately 10%. Another large part is the 30% error of $\sigma^{(2)}$ reported by Liu *et al.*[20] Other smaller uncertainties are due to the accuracy with which we were able to measure the beam waist, w_0, and the laser pulse length τ. The errors stated in Table I are root-mean-square values of all these contributions.

V. COMPARISON WITH A THEORETICAL MODEL

The results presented in Table I were derived from a first-order approximation under the assumption of negligible STE absorption during the interaction of KBr with the laser pulses. This assumption cannot be made *a priori*. For example, take the case of NaCl exposed to 532-nm pulses of 74 ps. In this situation the formation time (<5 ps) of STE's in the triplet state (the state which is responsible for the π luminescence) is significantly shorter than the pulse duration.[22] Since the triplet state has a strong absorption band centered at 2.15 eV,[23] encompassing the incident photon energy (2.33 eV), the STE's are very efficiently excited; as a consequence, their luminescence yield is reduced. This is probably the reason why our attempts to measure $\sigma^{(4)}$ in NaCl at 532 nm using STE recombination luminescence have been unsuccessful so far.

To independently check the reliability of our method for measuring the four-photon absorption cross section in KBr, we have developed a multiphoton absorption model similar to the one discussed by Brost *et al.*[12] to simulate the interaction of KBr with intense photon fields of 532 and 266 nm. The model consists of a set of rate equations (see Appendix B), which take into account all possible photon interaction processes in intrinsic KBr: four- or two-photon exciton generation, subsequent primary defect formation (e.g., STE's and V_k centers), absorption by and possible ionization of these primary defects, and, finally, their radiative or nonradiative decay. On the basis of the experimentally determined first-order approximation of the four- and two-photon absorption cross sections, this set of equations is solved for the total STE luminescence yields (π and σ) as a function of peak flux of the incident

TABLE I. Four-photon absorption cross-section measurements in KBr.

Sample	Boule area	$\frac{\eta_2}{\eta_4}$	w_{0g} (μm)	$\sigma^{(4)}$ (cm^8 sec^3)
1	top	0.90	6.2	$(4.5\pm1.9)\times10^{-112}$
2	top	0.85	8.5	$(1.7\pm0.7)\times10^{-112}$
3	bottom	0.93	8.3	$(0.8\pm0.3)\times10^{-112}$
4	bottom	0.93	8.5	$(0.6\pm0.3)\times10^{-112}$

laser pulses. The results are compared with the measured luminescence yields versus peak flux.

A. Two- and four-photon absorption models

A schematic representation of the relevant laser-induced electronic transitions in KBr is given in Fig. 5. The entire interaction process is governed by initial two- or four-photon absorption. Electron-hole pairs are generated as a result of this absorption. The holes bond rapidly (within 10^{-13} sec) (Ref. 22) to one of the nearest-neighbor Br^- ions forming so-called V_k centers (or self-trapped holes). These may be viewed as covalently bonded Br_2^- ions oriented along the $\langle 110 \rangle$ direction. The V_k center has a very large cross section for electron capture:[22] $\sigma = 2 \times 10^{-14}$ cm^2. Trapping of free electrons by V_k centers results in the formation of self-trapped excitons (STE's) in either the triplet ($^3\Sigma_u^+$) or the singlet ($^1\Sigma_u^+$) state with branching fractions of γ_3 and γ_1, respectively. At low temperature, the transitions, $^3\Sigma_u^+ \rightarrow {}^1\Sigma_g^+$ and $^1\Sigma_u^+ \rightarrow {}^1\Sigma_g^+$, give rise to the π and σ luminescence, respectively. The remaining portion (γ_0) of V_k-e pairs recombine nonradiatively through various channels back to the normal lattice configuration. The branching fractions are normalized: $\gamma_0 + \gamma_1 + \gamma_3 = 1$. In an intense photon field, the laser-generated V_k centers and STE's may absorb photons and ionize as indicated in Fig. 5. The results of the ionization will be discussed below.

We disregard here one recombination channel of the V_k-e pairs, namely F-H pair formation, and possible contributions to the free-carrier concentration caused by F-center ionization in the intense photon field. There are several reasons for this. The most important one is derived from the recent work by Williams *et al.*[24] These authors have identified the STE triplet state (which is responsible for the π luminescence in alkali halides) to be effectively a nearest-neighbor (or unstable) F-H pair because of nearly identical equilibrium lattice configurations

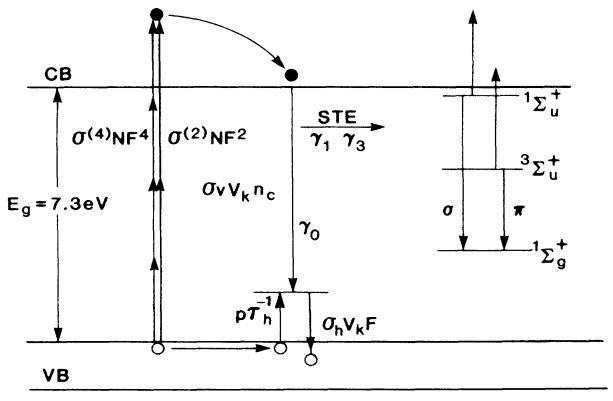

FIG. 5. Energy-level diagram for the possible electronic transitions. The electron-hole pairs are generated under either two- or four-photon excitation. The direct recombination channel is indicated by γ_0. Two additional channels exist for the formation of STE's in either π or σ states with branching fractions of γ_3 and γ_1, respectively. At low temperature these STE's decay to the ground state by emitting photons (π and σ luminescence).

of these two primary defect species. Since mutual annihilation of the unstable pair gives rise to the π luminescence, this F-H pair may simply be considered, for our purposes, a STE in the triplet state. On the other hand, only 2% of the F-H pairs remain stable at low temperature[25] by forming next-nearest-neighbor or further-separated F-H pairs. Their ionization, if any, will contribute negligibly to the free-carrier density and, hence, the STE luminescence yield. Therefore, we need only consider the V_k centers and STE's in the triplet and the singlet states.

B. Optical properties of V_k centers and STE's

V_k centers, considered to be perturbed diatomic molecular ions, have their own characteristic absorption spectrum.[26] In KBr three V_k absorption bands are observed at 3.22, 1.65, and 1.38 eV with full widths at half maximum of 0.73 and 0.26 eV for the first two bands, respectively.[26] At 532 and 266 nm the absorption stems mainly from the 3.22-eV band. This transition results in dissociation of the V_k center which immediately (within 10^{-13} sec) (Ref. 22) reforms with equal probability in one of the six equivalent $\langle 110 \rangle$ orientations.

The V_k-center absorption depends strongly upon the polarization of the incident light.[27] In our experimental arrangement, there are only three distinct orientations of V_k centers with respect to the polarization direction $\langle 110 \rangle$ of the incident light, which we distinguish as V_{k1}, V_{k2}, and V_{k3}. V_{k1} is parallel to $\langle 110 \rangle$, V_{k2} has its axis at a 60° angle to $\langle 110 \rangle$ (i.e., $\langle 101 \rangle$, and three other equivalent orientations), and V_{k3} is perpendicular to $\langle 110 \rangle$. The respective absorption cross sections are different. V_{k1} has the strongest absorption and V_{k3} the weakest. Assuming simple dipole transitions, we can estimate the relative values for the cross sections to be $\sigma_{h1} = 4\sigma_{h2}$ and $\sigma_{h3} = 0$. Using Smakula's formula with an oscillator strength of 0.75 and taking the width of the 3.22-eV V_k absorption band in KBr given by Delbecq *et al.*[26] to be the average value for V_{k1}, V_{k2}, and V_{k3}, we obtain the cross sections for V_{k1}, V_{k2}, and V_{k3} absorption (i.e., σ_{h1}, σ_{h2}, and σ_{h3}) at both 532 and 266 nm (see Appendix B, Table II).

The time for STE formation in the triplet state has been measured to be approximately 60 ps in KBr,[28] which is close to the laser pulse length (74 ps for 532 nm and 54 ps for 266 nm). Therefore, the interaction of STE's in the triplet state with incident photons during the pulse is expected to be relatively weak. The rise time of STE's in the singlet state is not known; but from its value for KI (Ref. 29 and 30) one would expect that it is shorter than 60 ps. The lifetime of STE's at 50 K, on the other hand, was estimated to be 0.8 μs for π and 0.7 ns for σ excitons.[31]

Williams *et al.*[23] measured the absorption spectrum of STE's in the triplet state and determined the transitions at 532 and 266 nm to be dominated by hole rather than electron excitation. We will assume in our model that hole absorption also occurs in the case of STE's in the singlet state. Because of this, a polarization dependence of STE absorption at 532 and 266 nm is expected as well. The values for the STE absorption cross sections in KBr at

both 266 and 532 nm should be, therefore, very close to those of V_k centers. However, an estimation on the basis of the spectrum given by Williams *et al.*[23] yields smaller cross sections (approximately one order of magnitude smaller than those for V_k centers at both 266 and 532 nm). In our calculation, we choose the π and σ STE absorption cross sections, σ_{3i} and σ_{1i}, to be $\sigma_{3i}=\sigma_{1i}=\sigma_{hi}/8$ at 532 nm, respectively, where i $(=1,2,3)$ denotes the three different orientations of STE's as in the case of V_k centers. At 266 nm, however, we simply use $\sigma_{3i}=\sigma_{1i}=\sigma_{hi}$ because of negligible STE absorption at this wavelength (see below). The values are listed in Table II, Appendix B.

The consequence of hole absorption by STE's is not well known. Ban *et al.*[32] found that in RbI hole absorption by STE's in the triplet state results in converting π excitons to σ excitons, which suggests a possible Auger-type transition. We assume this process to occur also in KBr.

C. STE luminescence efficiency

The total STE luminescence efficiency in KBr was estimated by Ikezawa *et al.* to be 0.12 photons per electron-hole pair at 11 K.[15] This result is not in agreement with our experimental observation of 0.41 photons per pair at 50 K. We attribute this to the difference in the ratio of the triplet to singlet luminescence intensities (or the branching ratio), which Ikezawa *et al.* found to be approximately 0.71 while we measure 2.7. We believe the reason for this discrepancy is due to the splitting of the π luminescence band into two at temperatures around 50 K.[33]

Under 266-nm excitation we observe an additional luminescence peak at temperatures above 40 K. With increasing temperature it shifts from its usual π peak site (2.28 eV) towards higher energy with a simultaneous increase in intensity. At lower temperature this peak overlaps the usual π peak. Its appearance considerably broadens the π band at 50 K and, as a consequence, increases the total π luminescence yield relative to the σ. This peak was first observed under x-ray excitation by Karasawa *et al.*[34] who speculated it to be a possible second π band. We also detect this shift under four-photon (532 nm) excitation.[33] The presence of this additional peak under three different excitations (two-photon four-photon, and x-ray) together with its optical properties strongly suggests that this additional emission band is an intrinsic STE luminescence band in KBr. The luminescence efficiency as well as the branching ratio of π to σ reported by Ikezawa *et al.*[15] might be based on one π peak (the 2.28-eV band) only because they employed a monochromator for detection, causing them to interpret the unrecognized shift of the second one out of the monitored-wavelength interval as a decrease in luminescence yield. In order to determine more accurately the STE luminescence efficiency in KBr at 50 K, we performed the following experiment.

It is known that the STE luminescence efficiency in KI at temperatures below 100 K is nearly unity.[35,36] This unique property allows one to determine the quantum yield of both π and σ luminescence in KBr by comparing them to the total STE luminescence yield generated under the same experimental conditions in KI and correcting them on the basis of the known absorption cross sections for exciton generation. Two-photon excitation at 266 nm was employed in this experiment together with the known two-photon absorption cross sections for both KI and KBr at 266 nm measured by Liu *et al.*[20] At this wavelength, the secondary absorption due to STE's is estimated to be negligible (see below), and, therefore, the yields of triplet and singlet luminescence reflect more closely the intrinsic efficiencies of STE luminescence rather than those influenced by redistribution.[12] The experimental arrangement was the same as that shown in Fig. 1. Two samples with approximately the same thickness were mounted vertically on the cold finger, one being on top of the other. One side of the samples was aligned properly so that the distance between the samples and the fiber was kept fixed to insure nearly identical collection efficiencies for both cases (note that for small numerical apertures, such as $A_N=0.2$, a slight difference in the refractive index affects the collection efficiency only very slightly). By moving the cold finger perpendicularly to the fiber, we were able to measure the STE luminescence from either KI or KBr without changing the experimental conditions. The luminescence signals obtained from single 266-nm laser pulses were averaged by fitting them to a proper two-photon model, i.e., $L=aE^2+b$, where L is the integrated STE luminescence yield, and a and b are constants. The efficiencies obtained for the π and σ luminescence in KBr are 0.30 and 0.11, respectively.

D. Computational results

With knowledge of all the parameters discussed above, we now proceed to calculate the STE luminescence yields as a function of flux under both four- and two-photon excitations. The method used for the calculation is similar to that employed by Brost *et al.*[12] The fluxes represent peak values. All spatially dependent entities are assigned

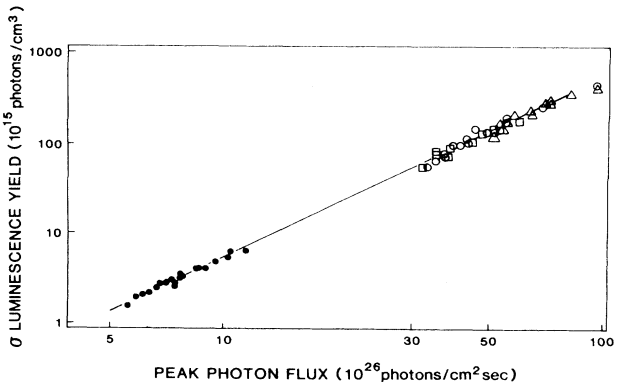

FIG. 6. Experimental and calculated dependence of the σ luminescence yield on incident photon flux under two-photon excitation. The experimental data points are normalized to the calculated curve (for details see text). The four different symbols for the data points represent those from four measurements.

their values at the geometrical focal point. The four-photon cross section used in the calculation is the averaged value obtained from the four separate measurements listed in Table I, while the two-photon absorption cross section is taken from Liu *et al.*[20] The calculated σ luminescence yields at the geometrical focal point as a function of incident photon flux are shown in Figs. 6 and 7 and compared with the experimental results.

In the two-photon case, the measured luminescence signals are normalized to the calculated curve by first converting them to peak values and then multiplying them by a proper factor to obtain the best fit to the calculated results. The first step is easily done by dividing all the luminescence signals by the fraction of the interaction volume V_{uv} visible to the fiber. The calculated curve (Fig. 6) exhibits a slope of 2.0 on a log-log scale, indicating that STE absorption at the fluxes used is negligible. The experimental results from four different measurements confirm this with slopes lying between 1.9 and 2.1. This suggests that the two-photon model can be simplified considerably by neglecting all STE absorption. This has been checked in the calculation, the difference in the total luminescence yields calculated with and without STE absorption being less than 0.002% at the photon fluxes used in the experiments.

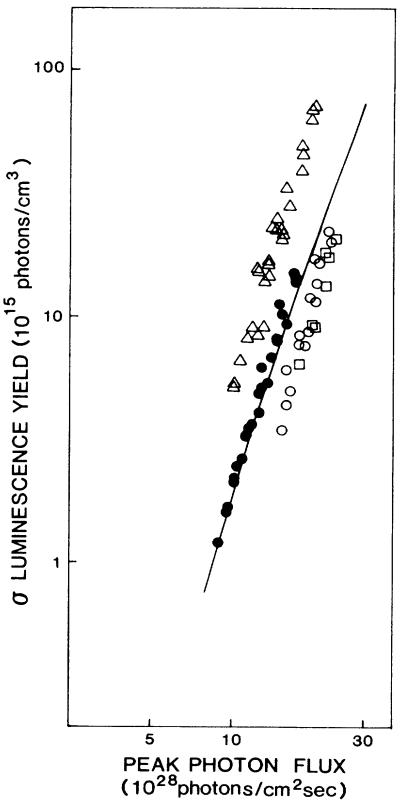

FIG. 7. Plot of experimental and calculated σ luminescence yields versus incident photon fluxes at geometrical focal point under four-photon excitation. The normalization procedure of the experimental data is given in the text. The calculated curve is obtained by using the mean cross section $\sigma^{(4)}=2\times10^{-112}$ cm^8 sec^3.

In Fig. 7 the four-photon data are presented, which are normalized in the following manner. First, we divide the luminescence signals by the interaction volume V_g to convert them to the peak values as is done in the two-photon case. Second, we multiply the peak values by the same normalization factor we determined to give the best fit in the two-photon case together with the calculated difference in the collection efficiency (η_2/η_4). According to Eq. (3), this normalization procedure should, in principle, give the first-order approximation of the integrated σ luminescence yield at the geometrical focal point under four-photon excitation as a function of the incident photon flux. The upper set of normalized data points in Fig. 7 is the one which yields a first-order $\sigma^{(4)}=4.5\times10^{-112}$ cm^8 sec^3, while the lower part of the data points (open circles, open squares) corresponds to $\sigma^{(4)}=0.8\times10^{-112}$ cm^8 sec^3 and 0.6×10^{-112} cm^8 sec^3, respectively. The agreement between the experimental and calculated results turns out to be very good considering such high-order nonlinear processes, and, more importantly, the calculated curve verifies the validity of the first-order approximation employed here for the calculation of $\sigma^{(4)}$ for KBr. The calculation also confirms the effect we observed, i.e., the slope of the STE luminescence versus incident photon flux curve on a log-log scale being less than four at higher fluxes.

To ensure that the decrease of the experimentally determined slope from four to a smaller value (Fig. 7) at higher fluxes was indeed caused by the STE ionization rather than by a temperature increase (which would decrease the STE luminescence efficiency[34]), we have further calculated the temperature change during the four-photon excitation using a temperature model (see Appendix B) similar to the ones developed by Braunlich *et al.*[13] and Jones.[16] The equation was solved for the temperature increase at the focal pont with the flux $F=3.2\times10^{29}$ photons/cm^2 sec (the highest one used in the experiments). The calculation indicates that the temperature rise was less than 8 K, which is still in the flat region of the measured σ luminescence versus temperature curve (this curve starts to decay at temperature above 60 K).[33] The calculation was performed assuming worst-case conditions using the specific heat obtained at 40 K. Therefore, we conclude here that the effect of the slopes being less than four is attributed to the ionization of STE's during their interaction with the laser pulses rather than a rise in temperature.

VI. SUMMARY

We have reported here a method of using STE recombination luminescence for the determination of the four-photon absorption cross section in KBr at 532 nm. We have verified the validity of this method by solving a set of appropriate kinetic equations (describing the interaction of 532-nm photon field with KBr at 50 K) to obtain the luminescence yield L_m as well as the rise in temperature

in the interaction volume as a function of laser photon flux F. Because of the high intensity of the photon field, STE absorption at 532 nm has slight effect on luminescence yield reducing the otherwise expected slope of 4 of the double-logarithmic plot L_m versus F. The effect of temperature increase on STE luminescence efficiency, on the other hand, is found to be negligible at photon fluxes up to 3.2×10^{29} photons/cm^2 sec. The four-photon absorption cross section measured for KBr at 532 nm is $\sigma^{(4)}=(2\pm1)\times10^{-112}$ cm^8 sec^3, which corresponds to a four-photon absorption coefficient, $\alpha^{(4)}=(2\pm1)\times10^{-7}$ cm^5 GW^{-3}.

ACKNOWLEDGMENTS

We would like to express our appreciation to Mr. Tom Casper for his valuable assistance. This work was supported by the National Science Foundation under Grant No. DMR-81-07099 and the Air Force Office of Scientific Research under Grant No. AFOSR-87-0081.

APPENDIX A: CALCULATION OF THE STE LUMINESCENCE COLLECTION EFFICIENCY

In this section we discuss the efficiency η_m for collecting the STE luminescence with an optical fiber. According to Eq. (3), not the absolute collection efficiency but only knowledge of the ratio η_2/η_4 is required. This allows us to disregard attenuation of the luminescence in the fiber, the throughput of the spectrograph, and the quantum efficiency of the optical multichannel analyzer, etc., all of which are identical for both excitation wavelengths. The only contribution to η_m we have to consider here stems from the difference in the spatial distribution of the STE luminescence intensities generated under excitation by pulses of the two different wavelengths. To appreciate this difference, we first calculate the probability function P for the fiber to collect and transmit a photon emitted from an arbitrary point inside the interaction volume.

The probability function is determined by two conditions: (a) a photon emitted from a source point must strike the input surface of the fiber, (b) the angle of incidence must be smaller than the critical angle α of the fiber (spatial steady-state approximation[37]). These two conditions define an acceptance area S on the fiber face for each source point. Only light within the solid angle subtended by the acceptance area (the solid angle of acceptance) can be transmitted by the fiber. Obviously this parameter is a function of the source location.

Assuming that photons are emitted randomly from the interaction site in all directions with equal probability, the probability function P is then related to the solid angle discussed above divided by 4π. For the nearly line-shaped interaction volumes in our experiments, P reduces to a function of z only [see Fig. 8(a)], and the acceptance area S can then be determined as follows.

For a source located at z the critical angle (in our case $\alpha=11.5°$) defines a cone which intercepts the fiber surface as shown in Fig. 8(b). The intercepted area (shaded) is the acceptance area of the fiber S which in our case is simply

$$S=\begin{cases}\pi a^2, & 0<z<a_m-a\\ S_1+S_2, & a_m-a<z<a_m+a\end{cases},$$

where

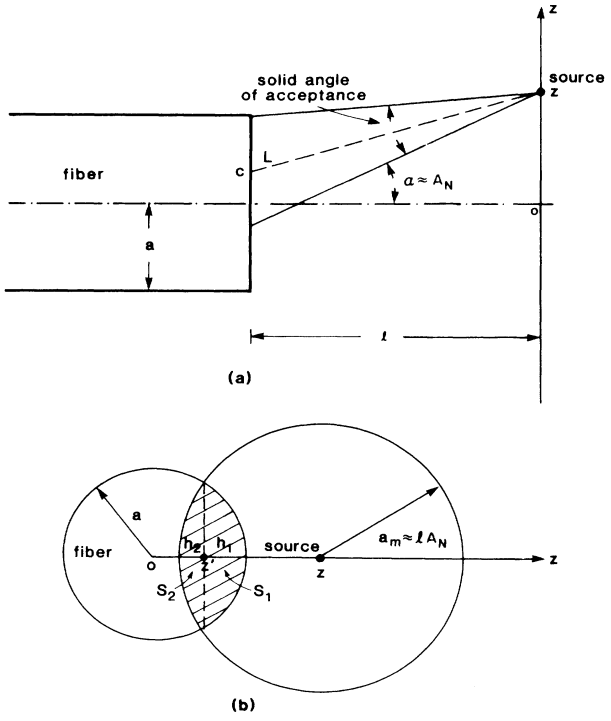

FIG. 8. (a) The solid angle of acceptance for a point source at z. L is the distance between the center of the acceptance area and the source position. (b) The acceptance area (shaded) of the fiber for a point source located at z.

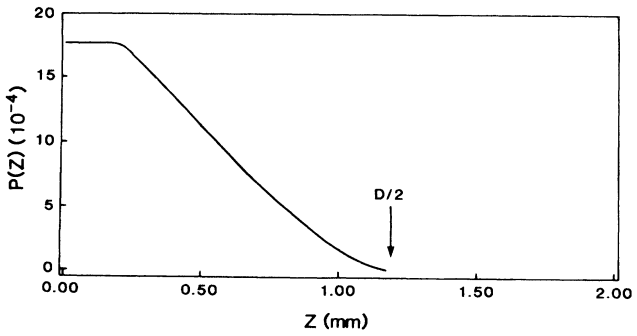

FIG. 9. The probability function $P(z)$ for a geometry in which $s=2.6$ mm, $d=1.4$ mm (compare Figs. 3 and 8).

$$S_1 = a^2 \cos^{-2}\left[\frac{a-h_1}{a}\right] - (a-h_1)(2ah_1 - h_1^2)^{1/2} ,$$

$$h_1 = a - z'$$

$$S_2 = a_m^2 \cos^{-1}\left[\frac{a_m - h_2}{a_m}\right] - (a_m - h_2)(2a_m h_2 - h_2^2)^{1/2} ,$$

$$h_2 = a_m - (z - z')$$

$$z' = -\frac{a_m^2 - a^2 - z^2}{2z} ,$$

and $a_m = lA_N$ [see Fig. 8(b)].

The probability function P is then [Fig. 8(a)]

$$P(z) = \begin{cases} \frac{1}{4\pi}\frac{Sl}{[l^2+z^2]^{3/2}}, & 0 < z < a_m - a \\ \frac{1}{4\pi}\frac{Sl}{L^3}, & a_m - a < z < a_m + a \end{cases}$$

where

$$L = [l^2 + \tfrac{1}{4}(z + a_m - a)^2]^{1/2} .$$

This function is symmetric with respect to the origin, $z = 0$.

Here, the equation for the probability function is derived by assuming that the emission occurs in vacuum. In a crystal, the solid angle of acceptance must be corrected for refraction. For small incident angles, this is done by replacing the optical distance $l = s + d$ (see Fig. 3) by $l = sn + d$, and dividing the numerical aperture of the fiber by the refractive index n of the crystal. Since the numerical aperture of the quartz collection fiber is only 0.2, the condition of small incident angles is easily met. A plot of the probability function $P(z)$ for a typical geometry of our experiment is given in Fig. 9.

The collection efficiency η_m is then simply

$$\eta_m = \frac{\int_0^{D/2} \frac{P(z)dz}{\left[1+\left[\frac{z}{z_0}\right]^2\right]^{m-1}}}{\int_0^{D/2} \frac{dz}{\left[1+\left[\frac{z}{z_0}\right]^2\right]^{m-1}}} ,$$

where

$$\frac{1}{\left[1+\left[\frac{z}{z_0}\right]^2\right]^{m-1}}$$

is the z dependence of the function

$$\int_0^{\infty}\int_0^{2\pi} F^m(\mathbf{r},t) r\, dr\, d\varphi$$

and D is defined in Sec. III.

Here we have only considered the case of $a_m > a$, or equivalently $l > a/A_N$. For the case $a_m < a$, $P(z)$ becomes

$$P(z) = \begin{cases} \frac{1}{4\pi}\frac{\pi a_m^2}{l^2}, & 0 < z < a - a_m \\ \frac{1}{4\pi}\frac{(S_1+S_2)l}{L^3}, & a - a_m < z < a + a_m \end{cases} .$$

All parameters are the same as those in the case of $a < a_m$. With known probability function $P(z)$ the parameter η_m can then be calculated numerically (see Table I).

APPENDIX B: RATE EQUATIONS

The following set of rate equations describes the formation of charge carriers and primary defects during the interaction of KBr with intense laser pulses of either 532- or 266-nm wavelength:

$$\frac{dn_c}{dt} = \sigma^{(m)} N F^m - \sigma v V_k n_c + \sum_{i=1}^{3} (\sigma_{3i} S_{3i} + \sigma_{1i} S_{1i}) F ,$$

$$\frac{dp}{dt} = \sigma^{(m)} N F^m - p\tau_h^{-1} + \sum_{i=1}^{3} \sigma_{hi} V_{ki} F ,$$

$$\frac{dV_{k1}}{dt} = \tfrac{1}{6} p\tau_h^{-1} - \sigma v V_{k1} n_c - \sigma_{h1} V_{k1} F + \tfrac{1}{6}\sum_{i=1}^{3} (\sigma_{3i} S_{3i} + \sigma_{1i} S_{1i}) F ,$$

$$\frac{dV_{k2}}{dt} = \tfrac{4}{6} p\tau_h^{-1} - \sigma v V_{k2} n_c - \sigma_{h2} V_{k2} F + \tfrac{4}{6}\sum_{i=1}^{3} (\sigma_{3i} S_{3i} + \sigma_{1i} S_{1i}) F ,$$

$$\frac{dV_{k3}}{dt} = \tfrac{1}{6} p\tau_h^{-1} - \sigma v V_{k3} n_c - \sigma_{h3} V_{k3} F + \tfrac{1}{6}\sum_{i=1}^{3} (\sigma_{3i} S_{3i} + \sigma_{1i} S_{1i}) F ,$$

$$\frac{dS_3}{dt} = \gamma_3 \sigma v V_k n_c - \sum_{i=1}^{3} \sigma_{3i} S_{3i} F - S_3 \tau_3^{-1} ,$$

$$\frac{dS_1}{dt} = \gamma_1 \sigma v V_k n_c - \sum_{i=1}^{3} \sigma_{1i} S_{1i} F - S_1 \tau_1^{-1} ,$$

$$L^{(3)} = \int_{-\infty}^{\infty} S_3 \tau_3^{-1} dt ,$$

and

$$L^{(1)} = \int_{-\infty}^{\infty} S_1 \tau_1^{-1} dt .$$

TABLE II. Symbols and parameter values in multiphoton absorption model.

n_c	Density of conduction electrons
p	Density of free holes
$V_k(V_{ki})$	Density of V_k centers; $V_k=\sum_{i=1}^{3} V_{ki}$
$S_3(S_{3i})$	Density of STE's in the triplet state; $S_3=\sum_{i=1}^{3} S_{3i}$
$S_1(S_{1i})$	Density of STE's in the singlet state; $S_1=\sum_{i=1}^{3} S_{1i}$
$i(=1,2,3)$	Three different orientations of V_k centers and STE's (see discussion in Sec. V)
$N=1.4\times10^{22}$ cm^{-3}	Density of active atoms (i.e., Br^- ions)
F	Incident photon flux
m	Order of multiphoton absorption
$v=10^7$ cm/sec	Average thermal velocity of free electrons[a]
$\sigma^{(2)}=5.4\times10^{-50}$ cm^4 sec	Two-photon absorption cross section[b]
$\sigma^{(4)}=2\times10^{-112}$ cm^8 sec^3	Four-photon absorption cross section
$\sigma=2\times10^{-14}$ cm^2	Cross section for electron capture by V_k centers[c]
$\sigma_{h1}=\begin{cases}1.0\times10^{-20}\text{ cm}^2\\8.0\times10^{-18}\text{ cm}^2\end{cases}$	V_{k1} center absorption cross section at $\begin{cases}266\text{ nm}\\532\text{ nm}\end{cases}$
$\sigma_{h2}=\begin{cases}2.5\times10^{-21}\text{ cm}^2\\2.0\times10^{-18}\text{ cm}^2\end{cases}$	V_{k2} center absorption cross section at $\begin{cases}266\text{ nm}\\532\text{ nm}\end{cases}$
$\sigma_{h3}=0$	V_{k3} center absorption cross section at both 266 and 532 nm
$\sigma_{31}=\begin{cases}1.0\times10^{-20}\text{ cm}^2\\1.0\times10^{-18}\text{ cm}^2\end{cases}$	Absorption cross section for S_{31} at $\begin{cases}266\text{ nm}\\532\text{ nm}\end{cases}$
$\sigma_{32}=\begin{cases}2.5\times10^{-21}\text{ cm}^2\\2.5\times10^{-19}\text{ cm}^2\end{cases}$	Absorption cross section for S_{32} at $\begin{cases}266\text{ nm}\\532\text{ nm}\end{cases}$
$\sigma_{33}=0$	Absorption cross section for S_{33} at both 266 and 532 nm
$\sigma_{11}=\begin{cases}1.0\times10^{-20}\text{ cm}^2\\1.0\times10^{-18}\text{ cm}^2\end{cases}$	Absorption cross section for S_{11} at $\begin{cases}266\text{ nm}\\532\text{ nm}\end{cases}$
$\sigma_{12}=\begin{cases}2.5\times10^{-21}\text{ cm}^2\\2.5\times10^{-19}\text{ cm}^2\end{cases}$	Absorption cross section for S_{12} at $\begin{cases}266\text{ nm}\\532\text{ nm}\end{cases}$
$\sigma_{13}=0$	Absorption cross section for S_{13} at both 266 and 532 nm
$\tau_h=10^{-13}$ sec	Lifetime of a free hole[c]
$\tau_3=0.8$ μs	Lifetime of an STE in the triplet state[d]
$\tau_1=0.7$ ns	Lifetime of an STE in the singlet state[d]
$\gamma_3=0.30$	Branching fraction for formation of STE's in the triplet state
$\gamma_1=0.11$	Branching fraction for formation of STE's in the singlet state
$\gamma_0=0.59$	Branching fraction for direct recombination of electron-hole pairs
$L^{(3)}$	Integrated π luminescence yield per unit volume
$L^{(1)}$	Integrated σ luminescence yield per unit volume

TABLE II. (*Continued*).

T	Temperature at geometrical focal point
$c=1.3\times10^{18}$ eV/gK	Specific heat of KBr at 40 K
$\rho=2.75$ g/cm^3	Mass density of KBr
$E_g=7.3$ eV	Band gap of KBr[e]
$\sigma_p=8.8\times10^{-20}$ cm^2	Polaron absorption cross section[f]
$\hbar\omega_g=2.33$ eV	Photon energy at 532 nm
$4\hbar\omega_g-E_g=2.02$ eV	Energy released by a four-photon generated electron relaxing to the bottom of conduction band
$\epsilon_h=1.5$ eV	Energy gained by lattice from formation of a V_k center[g]
$\hbar\omega_g-\epsilon_h=0.83$ eV	Energy gained by lattice from dissociation of a V_k center via photon absorption
$E_g-\epsilon_h=5.8$ eV	Energy gained by lattice from direct recombination of an electron-hole pair
$\epsilon_3=2.3$ eV	Energy released when a π exciton forms (or, depth of $^3\Sigma_u^+$ state below conduction band)[h]
$\epsilon_1=0.16$ eV	Energy released when a σ exciton forms (or, depth of $^1\Sigma_u^+$ state below conduction band)
$\epsilon_d=1.22$ eV	Energy gained by lattice from dissociation of a ground state ($^1\Sigma_g^+$) STE[i]
$\hbar\omega_g-\epsilon_3=0.03$ eV	Energy gained by lattice from relaxation of a "hot" electron generated under ionization of a π exciton
$\hbar\omega_g-\epsilon_1=2.17$ eV	Energy gained by lattice from relaxation of a "hot" electron generated under ionization of a σ exciton
$\frac{1}{6},\frac{4}{6},\frac{1}{6}$	Probabilities of V_{k1}, V_{k2} and V_{k3} formation per electron-hole pair, respectively

[a]See Ref. 13.
[b]See Ref. 20.
[c]See Ref. 22.
[d]See Ref. 31.
[e]See Ref. 38.
[f]See Ref. 39.
[g]See Ref. 40.
[h]See Ref. 23.
[i]See Ref. 16.

The parameters are defined in Table II. This set of equations is solved for the total σ luminescence yield $L^{(1)}$ as a function of peak laser flux, and the results are compared to the measured luminescence yields versus peak fluxes (see Sec. V).

The temperature rise in the interaction volume under four-photon excitation is estimated via the following rate equation (see Refs. 16 and 13):

$$\rho c\frac{dT}{dt}=(4\hbar\omega_g-E_g)\sigma^{(4)}NF^4+\hbar\omega_g\sigma_p n_c F+\epsilon_h p\tau_h^{-1}+(\hbar\omega_g-\epsilon_h)\sum_{i=1}^{3}\sigma_{hi}V_{ki}F+(E_g-\epsilon_h)\gamma_0\sigma v V_k n_c+\epsilon_3\gamma_3\sigma v V_k n_c$$
$$+\epsilon_1\gamma_1\sigma v V_k n_c+\epsilon_d(S_3\tau_3^{-1}+S_1\tau_1^{-1})+(\hbar\omega_g-\epsilon_3)\sum_{i=1}^{3}\sigma_{3i}S_{3i}F+(\hbar\omega_g-\epsilon_1)\sum_{i=1}^{3}\sigma_{1i}S_{1i}F\ .$$

[1]W. L. Smith, Opt. Eng. **17**, 489 (1978).
[2]S. Brawer, Phys. Rev. B **20**, 3422 (1979).
[3]M. Sparks, D. L. Mills, R. Warren, Y. Holstein, A. A. Maradudin, L. J. Sham, and D. F. King, Phys. Rev. B **24**, 3519 (1981).
[4]N. Bloembergen, IEEE J. Quantum Electron. **QE-10**, 375 (1974).
[5]A. S. Epifanov, IEEE J. Quantum Electron. **QE-17**, 2018 (1981).
[6]A. S. Epifanov, Zh. Eksp. Teor. Fiz. **76**, 617 (1979) [Sov. Phys.—JETP **49**, 309 (1979)].
[7]P. Braunlich, A. Schmid, and P. Kelly, Appl. Phys. Lett. **26**, 150 (1975).
[8]A. Schmid, P. Kelly, and P. Braunlich, Phys. Rev. B **16**, 4569 (1977).
[9]P. Kelly, A. Schmid, and P. Braunlich, Phys. Rev. B **20**, 815 (1979).
[10]Scott C. Jones, X. A. Shen, P. Braunlich, P. Kelly, and A. S. Epifanov, Phys. Rev. B **35**, 894 (1987).
[11]V. Nathan, A. H. Guenther, and S. S. Mitra, J. Opt. Soc. Am. B **2**, 294 (1985).
[12]G. Brost, P. Braunlich, and P. Kelly, Phys. Rev. B **30**, 4675 (1984).
[13]P. Braunlich, G. Brost, A. Schmid, and P. J. Kelly, IEEE J. Quantum Electron **QE-17**, 2034 (1981).
[14]M. N. Kabler, Phys. Rev. **136**, A1296 (1964).
[15]M. Ikezawa and T. Kojima, J. Opt. Soc. Jpn. **27**, 1551 (1969).
[16]Scott C. Jones, Ph.D. dissertation, Washington State University, Pullman, WA, 1986.
[17]A. Yariv, *Quantum Electronics* (Wiley, New York, 1975).
[18]A. H. Firester, M. E. Heller, and P. Sheng, Appl. Phys. Lett. **43**, 151 (1983).
[19]M. J. Soileau, W. E. Williams, and E. W. Van Stryland, in *Laser Induced Damage in Optical Materials*, edited by A. H. Guenther, D. Milam, and B. E. Newnam, Natl. Bur. Stand. (U.S.) Spec. Publ. No 669 (U.S. GPO, Washington, D.C., 1984), pp. 387–405.
[20]P. Liu, W. L. Smith, H. Lotem, J. H. Bechtel, N. Bloembergen, and R. S. Adhav, Phys. Rev. B **17**, 4620 (1978).
[21]I. M. Catalano, A. Cingolani, and A. Minafra, Opt. Commun. **5**, 212 (1972).
[22]R. T. Williams, J. N. Bradford, and W. L. Faust, Phys. Rev. B **18**, 7038 (1978).
[23]R. T. Williams and M. N. Kabler, Phys. Rev. B **9**, 1897 (1974).
[24]R. T. Williams, K. S. Song, W. L. Faust, and C. H. Leung, Phys. Rev. B **33**, 7232 (1986).
[25]Y. Kondo, M. Hirai, and M. Ueta, J. Phys. Soc. Jpn. **33**, 151 (1972).
[26]C. J. Delbecq, W. Hayes, and P. H. Yuster, Phys. Rev. **121**, 1043 (1961).
[27]M. N. Kabler, *Point Defects in Solids*, edited by J. H. Crawford, Jr. and L. M. Slifkin (Plenum, New York, 1972), Vol. 1.
[28]J. M. Ortega, Phys. Rev. B **19**, 3222 (1979).
[29]Y. Suzuki, H. Ohtani, and M. Hirai, J. Phys. Soc. Jpn. **48**, 1783 (1980).
[30]Y. Suzuki and M. Hirai, J. Phys. Soc. Jpn. **43**, 1679 (1977).
[31]S. Wakita, Y. Suzuki, H. Ohtani, S. Tagawa, and M. Hirai, J. Phys. Soc. Jpn. **50**, 3378 (1981).
[32]Y. Ban, K. Tanimura, and N. Itoh, Phys. Lett. **80A**, 53 (1980).
[33]X. A. Shen, Ph.D. dissertation, Washington State University, Pullman, WA 1987.
[34]T. Karasawa and M. Hirai, J. Opt. Soc. Jpn. **40**, 128 (1976).
[35]K. J. Teegarden, Phys. Rev. **105**, 1222 (1957).
[36]R. B. Murray and F. J. Keller, Phys. Rev. **137**, A942 (1965).
[37]A. W. Snyder and J. D. Love, *Optical Waveguide Theory* (Chapman and Hall, New York, 1983).
[38]D. Frohlich and B. Staginnus, Phys. Rev. Lett. **19**, 496 (1967).
[39]W. Huybrechts and J. Devreese, in *Elementary Excitations in Solids, Molecules and Atoms, Vol. B*, edited by J. Devreese, A. B. Kunz, and T. C. Collins (Plenum, New York, 1974).
[40]W. B. Fowler, in *Physics of Color Centers*, edited by W. B. Fowler (Academic, New York, 1968).